Efficient Inverse Isoparametric Mapping Algorithm for Whole-Body Computed Tomography Registration Using Deformations Predicted by Nonlinear Finite Element Modeling

Mao Li[1]
Intelligent Systems for Medicine Laboratory,
School of Mechanical Engineering,
The University of Western Australia,
M050, 35 Stirling Highway,
Crawley, Perth, Western Australia 6009, Australia
e-mail: mao.li@research.uwa.edu.au

Adam Wittek
Intelligent Systems for Medicine Laboratory,
School of Mechanical Engineering,
The University of Western Australia,
M050, 35 Stirling Highway,
Crawley, Perth, Western Australia 6009, Australia
e-mail: adam.wittek@uwa.edu.au

Karol Miller
Intelligent Systems for Medicine Laboratory,
School of Mechanical Engineering,
The University of Western Australia,
M050, 35 Stirling Highway,
Crawley, Perth, Western Australia 6009, Australia
e-mail: karol.miller@uwa.edu.au

Biomechanical modeling methods can be used to predict deformations for medical image registration and particularly, they are very effective for whole-body computed tomography (CT) image registration because differences between the source and target images caused by complex articulated motions and soft tissues deformations are very large. The biomechanics-based image registration method needs to deform the source images using the deformation field predicted by finite element models (FEMs). In practice, the global and local coordinate systems are used in finite element analysis. This involves the transformation of coordinates from the global coordinate system to the local coordinate system when calculating the global coordinates of image voxels for warping images. In this paper, we present an efficient numerical inverse isoparametric mapping algorithm to calculate the local coordinates of arbitrary points within the eight-noded hexahedral finite element. Verification of the algorithm for a nonparallelepiped hexahedral element confirms its accuracy, fast convergence, and efficiency. The algorithm's application in warping of the whole-body CT using the deformation field predicted by means of a biomechanical FEM confirms its reliability in the context of whole-body CT registration. [DOI: 10.1115/1.4027667]

Keywords: image registration, inverse isoparametric mapping, finite element method, hexahedral element

1 Introduction

Whole-body CT plays an important role in cancer diagnosis, therapy planning, and treatment [1–3]. It typically involves comparison of the images acquired for different postures/positions of a patient [2]. Before such comparison can be conducted, the images need to be aligned in a process known as nonrigid (as both rigid body motion and deformations are involved) image registration [4]. In the past nonrigid registration of CTs (and other radiographic image modalities) relied solely on image processing methods that predict the deformation field within the human body organs/tissues without taking into account the principles of mechanics governing deformations of such organs/tissues [2,4]. Such methods do not ensure plausibility of the predicted deformations and their accuracy tends to decrease when the differences between the source and target images become large due to articulated motion of the body segments and soft tissue deformations [4–6]. Therefore, biomechanical models, in which predicting the organs/tissue deformation is treated as a computational problem of solid mechanics, have been introduced [7–11]. In most practical cases, such models utilize the FEM [12] with isoparametric element formulation to solve sets of partial differential equations governing the deformation behavior of continua.

Efficient specialized finite element algorithms that facilitate real-time prediction of organ deformations for radiographic image registration are available [13,14]. However, relatively little effort has been devoted to creating efficient algorithms for warping the source image using the predicted deformations. In this study, we propose such an algorithm in the context of computation of soft body organs deformations using explicit dynamics finite element procedures with hexahedral elements for spatial discretization. We verify the algorithm on simple wedge geometry and present an example of its application in warping a CT scan of the human lungs in the context of whole-body CT registration.

2 Methods

2.1 Problem Formulation. The deformation field predicted using a FEM is described at the nodes of the computation grid (finite element mesh). Displacements and position/location of an arbitrary point within the discretized continuum are determined from the nodal displacements and coordinates through interpolation within the element using element shape functions. In this study, we use eight-noded hexahedral isoparametric elements in which the same shape functions are used for interpolation of positions and displacements [12]. The eight-noded hexahedron is regarded as the most efficient element type for nearly incompressible very soft continua, such as soft tissues when explicit time integration schedule is used [15].

Locations of the finite element mesh nodes are typically different from locations of centers of the voxels in the image. Therefore, interpolation using nodal positions must be performed for every voxel center in the image [16]. Such interpolation requires the information about coordinates of a voxel in the element's local coordinate system, and the local coordinates need to be determined from the voxel's known coordinates in the global coordinate system in a process referred to as inverse isoparametric mapping (Fig. 1).

Inverse isoparametric mapping has been previously addressed in the publications by our research group (Intelligent System for Medicine Laboratory) and by other researchers. For instance, in our previous study [16], we presented a robust implementation of an algorithm for inverse isoparametric mapping in the context of neuroimage (MIR) registration for image-guided neurosurgery. However, this implementation requires splitting of all hexahedral elements in the model into tetrahedrons. A comprehensive but relatively complex numerical algorithm for the inverse isoparametric mapping transformation verified for 2D and 3D finite elements was presented in Refs. [17,18]. In Ref. [19], a general solution for the inverse transformation in 2D was proposed, and a general

[1]Corresponding author.

Manuscript received December 6, 2013; final manuscript received April 22, 2014; accepted manuscript posted May 14, 2014; published online June 3, 2014. Assoc. Editor: David Corr.

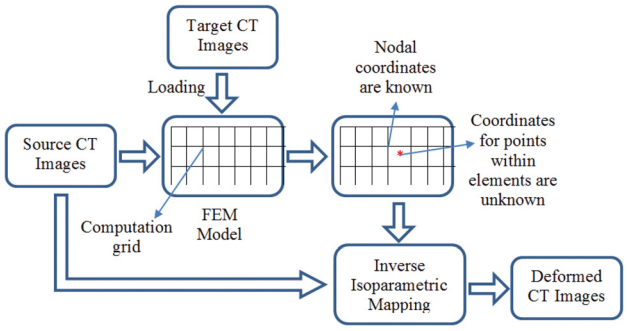

Fig. 1 A schematic diagram of warping the source whole-body CT images using the deformation field predicted by the patient-specific nonlinear finite element model

analytical expression of the inverse isoparametric relations for the linear hexahedral element was given in Ref. [20]. However, these approaches presented in the literature appear to be too complex for the problem considered in this study. The solution to inverse isoparametric mapping problem we proposed here is based on the numerical method using the Taylor's expansion presented in Ref. [21]. We selected this method for its simplicity, and the algorithm we introduce in this study further improves its efficiency.

2.2. Proposed Solution: Algorithm for Inverse Isoparametric Mapping. As explained in Sec. 2.1, we focus on isoparametric eight-noded hexahedral element as it is regarded as the most efficient element type for explicit integration of nearly incompressible very soft continua, such as soft tissues. As this element has been described and analyzed in numerous publications [22–24], here we provide only the key information necessary to explain our algorithm for inverse isoparametric mapping.

The global coordinates of an arbitrary point within a eight-noded hexahedral element are calculated using the following formula [12]:

$$x = \sum_{i=1}^{8} N_i x_i; \quad y = \sum_{i=1}^{8} N_i y_i; \quad z = \sum_{i=1}^{8} N_i z_i \tag{1}$$

where (x, y, z) are the global coordinates of an arbitrary point p belonging to the discretized continuum and (x_i, y_i, z_i) are the global coordinates of nodes (i.e., vertices of the element within which the point p is located), and N_i are the shape functions. For a eight-noded hexahedral element, the shape functions are [12]

$$N_i = \frac{1}{8}(1 + \xi\xi_i)(1 + \eta\eta_i)(1 + \varphi\varphi_i) \tag{2}$$

where (ξ, η, φ) and $(\xi_i, \eta_i, \varphi_i)$ are the local coordinates for a given point and nodes, respectively.

For the source configuration, the global nodal coordinates and global coordinates of the image voxels (defined as voxel centers) are known. For the deformed configuration, we predict the global nodal coordinates using a biomechanical FEM. From prediction, the global coordinates of the image voxels in the deformed configuration can be determined using Eqs. (1) and (2). This necessitates computation of the coordinates of the voxel centers in the element local coordinate system using the inverse coordinate transformation

$$\xi = \xi(x, y, z); \ \eta = \eta(x, y, z); \ \varphi = \varphi(x, y, z) \tag{3}$$

Given Eq. (2), the transformation defined by Eq. (3) is nonlinear. Therefore, using a numerical inverse isoparametric mapping method based on Taylor expansion presented in Ref. [21], we express the global coordinates of a voxel center (and any other arbitrary points) located within a given hexahedral element as follows:

$$\begin{aligned}
x_p &= x_0 + \left.\frac{\partial x}{\partial \xi}\right|_{(\xi_0,\eta_0,\varphi_0)} (\xi - \xi_0) + \left.\frac{\partial x}{\partial \eta}\right|_{(\xi_0,\eta_0,\varphi_0)} (\eta - \eta_0) + \left.\frac{\partial x}{\partial \varphi}\right|_{(\xi_0,\eta_0,\varphi_0)} (\varphi - \varphi_0) \\
y_p &= y_0 + \left.\frac{\partial y}{\partial \xi}\right|_{(\xi_0,\eta_0,\varphi_0)} (\xi - \xi_0) + \left.\frac{\partial y}{\partial \eta}\right|_{(\xi_0,\eta_0,\varphi_0)} (\eta - \eta_0) + \left.\frac{\partial y}{\partial \varphi}\right|_{(\xi_0,\eta_0,\varphi_0)} (\varphi - \varphi_0) \\
z_p &= z_0 + \left.\frac{\partial z}{\partial \xi}\right|_{(\xi_0,\eta_0,\varphi_0)} (\xi - \xi_0) + \left.\frac{\partial z}{\partial \eta}\right|_{(\xi_0,\eta_0,\varphi_0)} (\eta - \eta_0) + \left.\frac{\partial z}{\partial \varphi}\right|_{(\xi_0,\eta_0,\varphi_0)} (\varphi - \varphi_0)
\end{aligned} \tag{4}$$

In Eq. (4), the expansion takes place about a point with the global coordinates, (x_0, y_0, z_0) and $(\xi_0, \eta_0, \varphi_0)$, as the corresponding local coordinates. Equation (4) can be rewritten in a matrix form as

$$X_p = X_0 + J \cdot (\overline{\xi_p} - \overline{\xi_0}) \tag{5}$$

where J is the Jacobian matrix, and

$$\overline{\xi_p} = \overline{\xi_0} + J^{-1}(X_p - X_0) \tag{6}$$

where J^{-1} is the inverse of Jacobian matrix. Given Eqs. (5) and (6), for the global coordinates (of the voxel center) $X_p = (x_p, y_p, z_p)$, the corresponding local coordinates $\overline{\xi_p} = (\xi_p, \eta_p, \varphi_p)$ can be calculated using the following iterative algorithm:

$$\overline{\xi_{k+1}} = \overline{\xi_k} + J_k^{-1}(X_p - X_k) \ \ k = 0, 1, 2... \tag{7}$$

where $\overline{\xi_k}$ is the kth approximation for $\overline{\xi_p}$ and X_k are the global coordinates that correspond to $\overline{\xi_k}$. Termination criterion for iterations in Eq. (7) is defined using the L1 norm

$$|X_p - X_k| \le \varepsilon \tag{8}$$

where ε is the iteration convergence tolerance. In the examples shown here we used ε of 10^{-6} [21].

The number of voxels in a typical whole-body CT image is over 3×10^7, and biomechanical models applied to compute deformations for registrations of such images tend to consist of over 5×10^4 hexahedral elements [25]. As inverse of the Jacobian needs to be computed for every element of the mesh and local coordinates must be computed for every voxel in the image, the computational cost of numerical operations associated with Eq. (7) is substantial. To reduce this cost, we propose the following:

(1) Following Ref. [12], we notice that for eight-noded hexahedral elements, the Jacobian matrix can be expressed as

$$J=\begin{vmatrix}\frac{\partial x}{\partial\xi}&\frac{\partial y}{\partial\xi}&\frac{\partial z}{\partial\xi}\\ \frac{\partial x}{\partial\eta}&\frac{\partial y}{\partial\eta}&\frac{\partial z}{\partial\eta}\\ \frac{\partial x}{\partial\varphi}&\frac{\partial y}{\partial\varphi}&\frac{\partial z}{\partial\varphi}\end{vmatrix}=\begin{vmatrix}\frac{\partial N_1}{\partial\xi}&\frac{\partial N_2}{\partial\xi}&\cdots&\frac{\partial N_8}{\partial\xi}\\ \frac{\partial N_1}{\partial\eta}&\frac{\partial N_2}{\partial\eta}&\cdots&\frac{\partial N_8}{\partial\eta}\\ \frac{\partial N_1}{\partial\varphi}&\frac{\partial N_2}{\partial\varphi}&\cdots&\frac{\partial N_8}{\partial\varphi}\end{vmatrix}\cdot\begin{vmatrix}x_1&y_1&z_1\\ &\cdots&\\ x_8&y_8&z_8\end{vmatrix} \tag{9}$$

where $(\partial N_i/\partial\xi_j)(i=1,2,\cdots 8;\ \xi_j=\xi,\eta,\varphi)$ is the derivative of element shape functions with respect to local coordinates, $(x_i,y_i,z_i)\ i=1,2\cdots 8$ are the global nodal coordinates of a hexahedral element. Substituting Eq. (2) for N_i into Eq. (9), the derivatives of shape functions at the origin (0, 0, 0) of the element local coordinate system are

$$\begin{vmatrix}\frac{\partial N_1}{\partial\xi}&\frac{\partial N_2}{\partial\xi}&\cdots&\frac{\partial N_8}{\partial\xi}\\ \frac{\partial N_1}{\partial\eta}&\frac{\partial N_2}{\partial\eta}&\cdots&\frac{\partial N_8}{\partial\eta}\\ \frac{\partial N_1}{\partial\varphi}&\frac{\partial N_2}{\partial\varphi}&\cdots&\frac{\partial N_8}{\partial\varphi}\end{vmatrix}=\frac{1}{8}\begin{vmatrix}\xi_1&\xi_2&\cdots&\xi_8\\ \eta_1&\eta_2&\cdots&\eta_8\\ \varphi_1&\varphi_2&\cdots&\varphi_8\end{vmatrix} \tag{10}$$

where $(\xi_i,\eta_i,\varphi_i)\ i=1,2\cdots 8$ are the local nodal coordinates of the isoparametric hexahedral element. As for eight-noded hexahedral elements, the local nodal coordinates are (for convention of node numbering see Fig. 2)

$$\begin{vmatrix}\xi_1&\xi_2&\cdots&\xi_8\\ \eta_1&\eta_2&\cdots&\eta_8\\ \varphi_1&\varphi_2&\cdots&\varphi_8\end{vmatrix}=\begin{vmatrix}1,&1,&1,&1,&-1,&-1,&-1,&-1\\ -1,&1,&1,&-1,&-1,&1,&1,&-1\\ 1,&1,&-1,&-1,&1,&1,&-1,&-1\end{vmatrix} \tag{11}$$

$$\begin{aligned}\frac{\partial x}{\partial\xi}&=\frac{1}{2}\left\{\frac{1}{4}[(x_1-x_5)+(x_2-x_6)+(x_3-x_7)+(x_4-x_8)]\right\}=\frac{1}{2}l_{x\xi}\\ \frac{\partial y}{\partial\eta}&=\frac{1}{2}\left\{\frac{1}{4}[(y_2-y_1)+(y_3-y_4)+(y_6-y_5)+(y_7-y_8)]\right\}=\frac{1}{2}l_{y\eta}\\ \frac{\partial z}{\partial\varphi}&=\frac{1}{2}\left\{\frac{1}{4}[(z_1-z_4)+(y_2-y_3)+(y_5-y_8)+(y_6-y_7)]\right\}=\frac{1}{2}l_{z\varphi}\end{aligned} \tag{12}$$

and

$$\begin{aligned}\frac{\partial y}{\partial\xi}&=\frac{1}{2}\left\{\frac{1}{4}[(y_1-y_5)+(y_2-y_6)+(y_3-y_7)+(y_4-y_8)]\right\}=\frac{1}{2}l_{y\xi}\\ \frac{\partial z}{\partial\xi}&=\frac{1}{2}\left\{\frac{1}{4}[(z_2-z_1)+(z_3-z_4)+(z_6-z_5)+(z_7-z_8)]\right\}=\frac{1}{2}l_{z\xi}\end{aligned} \tag{13}$$

(2) If a eight-noded hexahedral element remains rectangular parallelepiped, $l_{y\xi}$, $l_{z\xi}$, $l_{x\eta}$, $l_{z\eta}$, $l_{x\varphi}$, and $l_{y\varphi}$ are equal to 0, and the Jacobian matrix for such element is

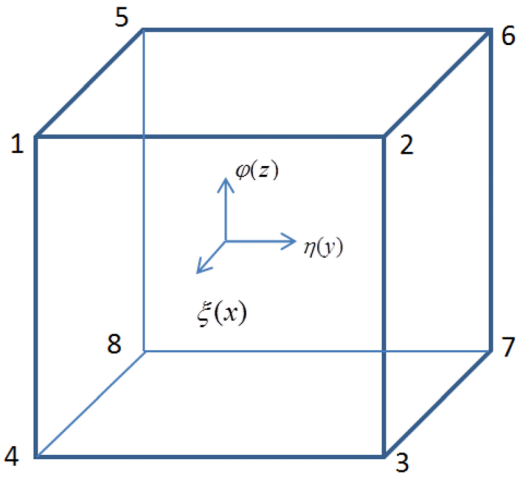

Fig. 2 The numbering system for the isoparametric hexahedral element

$$J^*=\frac{1}{2}\begin{vmatrix}l_{x\xi}&0&0\\ 0&l_{y\eta}&0\\ 0&0&l_{z\varphi}\end{vmatrix} \tag{14}$$

where the superscript * means this formula is exact for rectangular parallelepiped eight-noded hexahedral elements.

(3) Given Eq. (14), the local coordinates calculated by Eq. (6), can be written as

$$\overline{\xi_p^*}=\overline{\xi_0^*}+\left(X_p^*-X_0^*\right)./L \tag{15}$$

where the operator ./ means element-wise division, and

$$L=\frac{1}{2}\begin{vmatrix}l_{x\xi}\\ l_{y\eta}\\ l_{z\varphi}\end{vmatrix} \tag{16}$$

(4) For finite element meshes (Fig. 3) used in biomechanical models for computing the deformations for whole-body radiographic image registration, the vast majority of the elements are general hexahedrons rather than rectangular parallelepipeds. For such elements, the Jacobian matrix (Eq. (14)) is not diagonal (i.e., elements $l_{y\xi}$, $l_{z\xi}$, $l_{x\eta}$, $l_{z\eta}$, $l_{x\varphi}$, and $l_{y\varphi}$ may be nonzero) and Eq. (15) is not satisfied. However, as matrix inversion is computationally expensive, we do not use the exact inverse of the Jacobian matrix. Instead, we approximate the inverse using the following iterative formula derived from Eq. (15):

$$\overline{\xi_{k+1}}=\overline{\xi_k}+(X_p-X_k)\cdot/L\quad k=0,1,2... \tag{17}$$

where L is a vector which contains only the diagonal elements in the Jacobian matrix (Eq. (14)) and X_k is the kth approximation for X_p. Convergence of the iterative formula given by Eq. (17) is evaluated in Sec. 3.1 against a very stringent tolerance criterion.

(5) As in any iterative algorithm, the estimation of the initial value (i.e., initial local coordinates $\overline{\xi_{\text{Init}}}$) for Eq. (17) is of key importance as it tends to determine the number of iterations needed and associated computational cost. For an

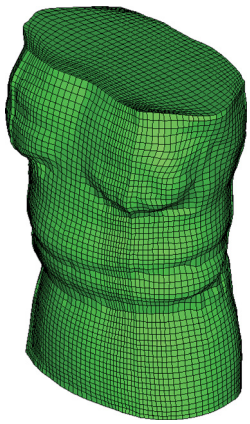

Fig. 3 The whole-body finite element model

isoparametric element, the local coordinates of any point within the element must be between −1 and 1, and coordinates $(0,0,0)$ are at the centroid. Therefore, for the eight-noded hexahedral element with shape functions given by Eq. (2), we propose to use the following formula to estimate the initial local coordinates $\overline{\xi_{\text{Init}}}$ for the iterative algorithm defined by Eq. (17):

$$\overline{\xi_{\text{Init}}} = (X_p - X_{\text{Centre}})./L \tag{18}$$

where X_{Centre} is the centroid of the hexahedral element which contains a given point (voxel center) X_p.

3 Results

3.1 Convergence of the Proposed Iterative Algorithm. To evaluate the convergence of the proposed iterative numerical inverse isoparametric mapping algorithm, a wedge-shaped continuum with brain tissue-like mechanical properties (the Neo-Hookean hyperelastic model with Young's modulus of 1000 Pa and Poisson's ratio of 0.495 [26]) discretized using eight-noded hexahedral elements that forming not rectangular parallelepiped was subjected to the imposed displacement on its top surface (Fig. 4(*a*)). The magnitude of displacements was 20% of the wedge height. Computation of the deformation field within the continuum was performed using a total Lagrangian explicit dynamic algorithm that we have previously developed and verified in numerous applications in image-guided surgery [13,27,28]. The predicted shape of the wedge due to the prescribed displacements is shown in Fig. 4(*b*).

We select a hexahedral element from the mesh shown in Fig. 4(*a*) and place three points in the element at locations defined by arbitrarily selected sets of global coordinates (−0.4883, −0.4000, 1.0000), (−0.4267, −0.3111, 1.0000), and (−0.4736, −0.3688, 0.9513) (Fig. 5(*a*)): Two points are located at the edges of the element and one in element interior. The corresponding point positions in the deformed element are calculated using the proposed algorithm as shown in Fig. 5(*b*). Even though the element undergoes serious distortion, the points initially located on the edges remain there.

From Table 1, it can be seen that despite substantial changes in the element geometry caused by the prescribed displacements, for the convergence tolerance of 10^{-6}, only up to seven steps were sufficient for our algorithm (Eq. (17)) to provide converged solution for coordinates of points P1, P2, and P3 (Fig. 5).

Table 1 indicates that for our inverse mapping algorithm convergence implies accuracy. For all the analyzed points, at the final iteration step (converged solution), the global coordinates calculated using local coordinates predicted by our algorithm could not be distinguished from the actual global coordinates within the numerical precision used.

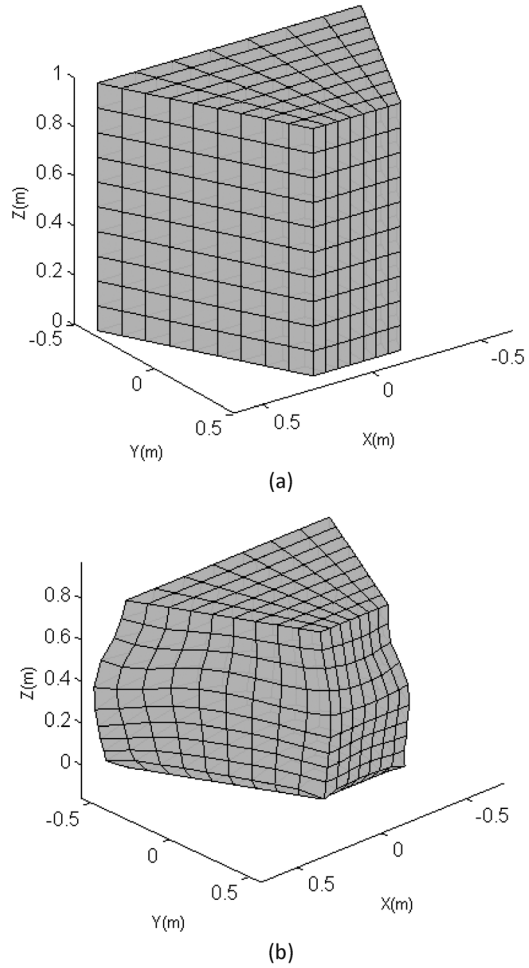

Fig. 4 A wedge-shaped continuum discretized by hexahedral elements: (*a*) the undeformed wedge-shaped geometry and (*b*) the wedge-shaped geometry is deformed by an imposed displacement on the top surface

Furthermore, the results presented in Table 2 suggest that the computation time for the algorithm given by Eq. (17) is appreciably reduced (by 40–60%) in comparison with that of the mapping algorithm using the exact inverse Jacobian matrix (Eq. (7)).

3.2. Application Example: Warping of Lung CT Image. The whole-body CT image dataset analyzed here is for Case #20 from the National Alliance for Medical Image Computing (NAMIC) Registration Library (http://www.na-mic.org/Wiki/index.php/Projects:RegistrationLibrary:RegLib_C20b).

Deformations within the patient's organs/soft tissue resulting from posture differences when acquiring set 1 (source image) and set 2 (target image) have been previously computed by us [25] using the FEM shown in Fig. 1. As the deformations are given at the nodes of the mesh shown in Fig. 3, we apply our inverse mapping algorithm given by Eq. (17) to each voxel of image set 1 to warp the source image to the geometry depicted in the target image.

When evaluating the warping accuracy and performance of our inverse mapping algorithm, we compare the predicted (i.e., warped using the predicted deformations) surface of the lungs with the actual surface extracted from the target image. The lungs were selected as they are a large body organ with boundaries clearly visible/easy to distinguish in both sets of CT images we analyzed here. As shown in Fig. 6, the predicted (deformed) and

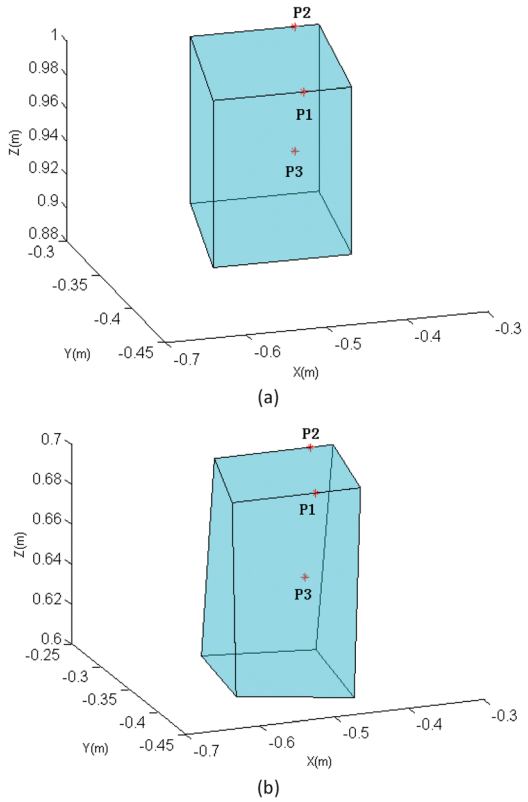

Fig. 5 Inverse isoparametric mapping transformation for a hexahedral element. (*a*) Three arbitrary points are placed in an undeformed hexahedral element and (*b*) the corresponding positions of these three points within a deformed element are calculated using the proposed inverse isoparametric mapping algorithm.

actual (target) (i.e., extracted from the target image) lung contours align very well, and the differences between them are within two voxels size of the image.

Table 2 Computation time (in seconds) for the inverse mapping algorithm (converged solution) we proposed in this study and the algorithm using exact form of the inverse Jacobian matrix for the example shown in Fig. 5

	Point 1	Point 2	Point 3
The algorithm using exact form of the inverse Jacobian matrix	6.36×10^{-4}	6.28×10^{-4}	5.73×10^{-4}
Proposed algorithm	3.61×10^{-4}	3.32×10^{-4}	3.35×10^{-4}

4 Discussions and Conclusions

Application of the organ deformations predicted by means of biomechanical models utilizing the FEM with isoparametric element formulation in image registration requires inverse mapping to determine voxels coordinates in local coordinate system and compute the global coordinates of the voxels in the deformed (target) image configuration. When conducting registration of whole-body radiographic images that consist of dozens of millions of voxels, the computational cost of this operation tends to be high. Therefore, in this study, we propose an iterative algorithm that reduces the computational cost of inverse parametric mapping in the context of whole-body CT registration.

To verify the proposed algorithm, we applied it to compute the internal coordinates of arbitrarily selected points located at the edges and within the nonparallelepiped hexahedral element extracted from a mesh of soft wedge-shaped continuum undergoing compression due to externally applied load (Fig. 4). The results indicate that the proposed algorithm converges quickly (within 6–7 iteration steps) and requires less computation time than the algorithm using the exact form of the inverse Jacobian matrix (i.e., 40% for the case that the point is within the element while 60% for the case that the points are at the edges/surfaces, as shown in Table 2). Similar improvement in the computational efficiency (around 30% reduction in the computation time) was achieved when applying our algorithm to warp the whole-body CT images (see Sec. 3.2).

In the proposed algorithm, the inverse mapping is applied to each voxel of the source image independently (i.e., computations

Table 1 Convergence performance of the inverse mapping algorithm we proposed in this study when solving the example shown in Fig. 5. Exact values of the global coordinates are in parentheses.

	Global coordinates of point 1 (−0.4883, −0.4000, 1.0000)		Global coordinates of point 2 (−0.4267, −0.3111, 1.0000)		Global coordinates of point 3 (−0.4736, −0.3688, 0.9513)	
	Local $\overline{\xi_k}$	Global X_k	Local $\overline{\xi_k}$	Global X_k	Local $\overline{\xi_k}$	Global X_k
Estimation of initial values of coordinates to start the iteration	0.0683 −1.0000 1.0000	−0.5084 −0.4000 1.0000	0.3197 −0.9997 1.0000	−0.4508 −0.3111 1.0000	0.2130 −0.2980 0.0260	−0.4831 −0.3688 0.9513
Iteration step 1	0.3122 −1.1045 1.0000	−0.4894 −0.4046 1.0000	0.6362 −1.1354 1.0000	−0.4280 −0.3171 1.0000	0.3285 −0.3475 0.0260	−0.4744 −0.3710 0.9513
Iteration step 2	0.3257 −1.0058 1.0000	−0.4865 −0.4003 1.0000	0.6533 −1.0071 1.0000	−0.4245 −0.3114 1.0000	0.3380 −0.3021 0.0260	−0.4728 −0.3690 0.9513
Iteration step 3	0.3036 −0.9905 1.0000	−0.4881 −0.3996 1.0000	0.6207 −0.9984 1.0000	−0.4269 −0.3110 1.0000	0.3279 −0.2937 0.0260	−0.4735 −0.3686 0.9513
…	…	…	…	…	…	…
Iteration step 6	0.3011 −0.9989 1.0000	−0.4885 −0.4000 1.0000	0.6233 −1.0009 1.0000	−0.4267 −0.3112 1.0000	0.3272 −0.2980 0.0260	−0.4736 −0.3688 0.9513
Iteration step 7	0.3032 −1.0000 1.0000	−0.4883 −0.4000 1.0000	0.6235 −0.9998 1.0000	−0.4267 −0.3111 1.0000	–	–

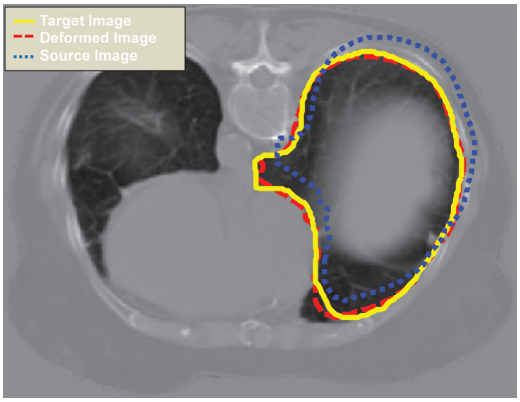

Fig. 6 Results of application of the proposed inverse mapping algorithm in registration/warping of a whole-body CT image set. A typical section through the registered image showing the lungs. Deformations between the source and target images for the registration were previously obtained in our previous study using nonlinear finite element procedures [23]. From the computed deformations, the registered/warped image was created by applying the proposed inverse isoparametric mapping algorithm to every voxel of the source images. The dotted line and the solid line are the lung contours in source and target images, respectively. The dashed line is the lung contour in the registered/warped image. It can be clearly seen that the contour obtained through registration of the source image agrees very well with the actual/"true" contour in the target image.

applied to a given voxel do not depend on the computations for other voxels) using the iterative formula given in Eq. (17). Therefore, the algorithm can be easily parallelized. Our experience in application of explicit nonlinear finite element procedures in computation of brain deformations due to surgery indicates that for algorithms exhibiting such features, orders of magnitude improvement in computational efficiency can achieved through the algorithm implementation on a graphics processing unit (GPU). Such implementation allows parallel computation using hundreds of cores available on GPU [29]. Therefore, we are confident that further significant improvement of computational speed of inverse mapping algorithm can be achieved using GPU.

Reliability of the proposed algorithm in the context of whole-body CT registration is confirmed by the results obtained when applying the algorithm to warp the whole-body CT acquired in the source configuration to the target CT geometry using the deformation field predicted by means of a biomechanical FEM (Fig. 6).

Acknowledgment

The first author is a recipient of the SIRF scholarship and acknowledges the financial support of the University of Western Australia. The Australian Research Council (Discovery Grant DP120100402) is gratefully acknowledged. The whole-body CT image dataset analyzed in this study was acquired from publically available Registration Library by National Center for Biomedical Computing (NA-MIC). NA-MIC is a national research center supported by grant U54 EB005149 from the NIBIB NIH HHS Roadmap for Medical Research Program.

References

[1] Sint Jan, S. V., Sobzack, S., Dugailly, P.-M., Feipel, V., Lefevre, P., Lufimpadio, J.-L., Salvia, P., Viceconti, M., and Rooze, M., 2006, "Low-Dose Computed Tomography: A Solution for in Vivo Medical Imaging and Accurate Patient-Specific 3D Bone Modeling?," Clin. Biomech., **21**(9), pp. 992–998.
[2] Lee, Y. S., Kim, K. J., Do Ahn, S., Choi, E. K., Kim, J. H., Lee, S. W., Song, S. Y., Yoon, S. M., Kim, Y. S., Park, J. H., Cho, B. C., and Kim, S. S., 2013, "The Application of PET-CT to Post-Mastectomy Regional Radiation Therapy Using a Deformable Image Registration," Radiat. Oncol., **8**, p. 104–113.
[3] Zaidi, H., 2007, "Optimisation of Whole-Body PET/CT Scanning Protocols," Biomed. Imaging Intervention J., **3**(2), p. e36–44.
[4] Li, X., Yankeelov, T. E., Peterson, T. E., Gore, J. C., and Dawant, B. M., 2008, "Automatic Nonrigid Registration of Whole Body CT Mice Images," Med. Phys., **35**(4), pp. 1507–1520.
[5] Mostayed, A., Garlapati, R. R., Joldes, G. R., Wittek, A., Roy, A., Kikinis, R., Warfield, S. K., and Miller, K., 2013, "Biomechanical Model as a Registration Tool for Image-Guided Neurosurgery: Evaluation Against BSpline Registration," Ann. Biomed. Eng., **41**(11), pp. 2409–2425.
[6] Wittek, A., Miller, K., Kikinis, R., and Warfield, S. K., 2007, "Patient-Specific Model of Brain Deformation: Application to Medical Image Registration," J. Biomech., **40**(4), pp. 919–929.
[7] Hagemann, A., Rohr, K., Stiehl, H. S., Spetzger, U., and Gilsbach, J. M., 1999, "Biomechanical Modeling of the Human Head for Physically Based, Nonrigid Image Registration," IEEE Trans. Med. Imaging, **18**(10), pp. 875–884.
[8] Otoole, R. V., Jaramaz, B., Digioia, A. M., Visnic, C. D., and Reid, R. H., 1995, "Biomechanics for Preoperative Planning and Surgical Simulations in Orthopedics," Comput. Biol. Med., **25**(2), pp. 183–191.
[9] Rohlfing, T., Maurer, C. R., O'Dell, W. G., and Zhong, J. H., 2004, "Modeling Liver Motion and Deformation During the Respiratory Cycle Using Intensity-Based Nonrigid Registration of Gated MR Images," Med. Phys., **31**(3), pp. 427–432.
[10] Snedeker, J. G., Wirth, S. H., and Espinosa, N., 2012, "Biomechanics of the Normal and Arthritic Ankle Joint," Foot Ankle Clin., **17**(4), pp. 517–528.
[11] Garlapati, R. R., Roy, A., Joldes, G. R., Wittek, A., Mostaryed, A., Doyle, B., Warfield, S. K., Kikinis, R., Knuckey, N., Bunt, S., and Miller, K., 2013, "Biomechanical Modeling Provides More Accurate Data for Neuronavigation Than Rigid Registration," J. Neurosurg. (in press).
[12] Bathe, K.-J., 1996, *Finite Element Procedures*, Prentice Hall, Englewood Cliffs, NJ.
[13] Joldes, G. R., Wittek, A., and Miller, K., 2009, "Suite of Finite Element Algorithms for Accurate Computation of Soft Tissue Deformation for Surgical Simulation," Med. Image Anal., **13**(6), pp. 912–919.
[14] Lerotic, M., Lee, S. L., Keegan, J., and Yang, G. Z., 2009, "Image Constrained Finite Element Modelling for Real-Time Surgical Simulation and Guidance," IEEE International Symposium on Biomedical Imaging From Nano to Macro, Boston, MA, pp. 1063–1066.
[15] Wittek, A., Joldes, G., and Miller, K., 2011, "Algorithms for Computational Biomechanics of the Brain," *Biomechanics of the Brain*, K. Miller, ed., Springer, New York, pp. 189–219.
[16] Joldes, G., Wittek, A., Warfield, S. K., and Miller, K., 2012, "Performing Brain Image Warping Using the Deformation Field Predicted by a Biomechanical Model," *Computational Biomechanics for Medicine*, P. M. F. Nielsen, A. Wittek, and K. Miller, eds., Springer, New York, pp. 89–96.
[17] Murti, V., and Valliappan, S., 1986, "Numerical Inverse Isoparametric Mapping in Remeshing and Nodal Quantity Contouring," Comput. Struct., **22**(6), pp. 1011–1021.
[18] Murti, V., Wang, Y., and Valliappan, S., 1988, "Numerical Inverse Isoparametric Mapping in 3D FEM," Comput. Struct., **29**(4), pp. 611–622.
[19] Hua, C., 1990, "An Inverse Transformation for Quadrilateral Isoparametric Elements: Analysis and Application," Finite Elem. Anal. Des., **7**(2), pp. 159–166.
[20] Yuan, K. Y., Huang, Y. S., Yang, H. T., and Pian, T. H. H., 1994, "The Inverse Mapping and Distortion Measures for 8-Node Hexahedral Isoparametric Elements," Comput. Mech., **14**(2), pp. 189–199.
[21] Qian, X. D., Ren, Q. W., and Zhao, Y., 1998, "An Algorithm for Inverse Isoparametric Mapping in FEM," Chin. J. Comput. Mech., **15**, pp. 437–440.
[22] Areias, P. M. A., de Sa, J. M. A. C., Antonio, C. A. C., and Fernandes, A. A., 2003, "Analysis of 3D Problems Using a New Enhanced Strain Hexahedral Element," Int. J. Numer. Methods Eng., **58**(11), pp. 1637–1682.
[23] Irving, G., Teran, J., and Fedkiw, R., 2006, "Tetrahedral and Hexahedral Invertible Finite Elements," Graph Models, **68**(2), pp. 66–89.
[24] Nagrath, S., Jansen, K. E., and Lahey, R. T., 2005, "Computation of Incompressible Bubble Dynamics With a Stabilized Finite Element Level Set Method," Comput. Method Appl. Mech. Eng., **194**(42–44), pp. 4565–4587.
[25] Li, M., Wittek, A., Joldes, G., Zhang, G., Dong, F., Kikinis, R., and Miller, K., 2013, "Whole-Body Image Registration Using Patient-Specific Non-Linear Finite Element Model," *Computational Biomechanics for Medicine: Fundamental Science and Patient-Specific Application*, B. J. Doyle, K. Miller, A. Wittek, and P. M. F. Nielsen, eds., Springer, New York, pp. 87–99.
[26] Miller, K., 2011, *Biomechanics of the Brain*, Springer, New York.
[27] Miller, K., Joldes, G., Lance, D., and Wittek, A., 2007, "Total Lagrangian Explicit Dynamics Finite Element Algorithm for Computing Soft Tissue Deformation," Commun. Numer. Methods Eng., **23**(2), pp. 121–134.
[28] Wittek, A., Joldes, G., Couton, M., Warfield, S. K., and Miller, K., 2010, "Patient-Specific Non-Linear Finite Element Modelling for Predicting Soft Organ Deformation in Real-Time: Application to Non-Rigid Neuroimage Registration," Prog. Biophys. Mol. Biol., **103**(2–3), pp. 292–303.
[29] Joldes, G. R., Wittek, A., and Miller, K., 2010, "Real-Time Nonlinear Finite Element Computations on GPU—Application to Neurosurgical Simulation," Comput. Methods Appl. Mech. Eng., **199**(49–52), pp. 3305–3314.